Optically induced transport through semiconductor-based molecular electronics

Guangqi Li, Boris D. Fainberg, and Tamar Seideman

Citation: The Journal of Chemical Physics **142**, 154111 (2015); doi: 10.1063/1.4917029
View online: http://dx.doi.org/10.1063/1.4917029
View Table of Contents: http://scitation.aip.org/content/aip/journal/jcp/142/15?ver=pdfcov
Published by the AIP Publishing

Optically induced transport through semiconductor-based molecular electronics

Guangqi Li,[1] Boris D. Fainberg,[2,3,a)] and Tamar Seideman[1,b)]
[1]*Department of Chemistry, Northwestern University, Evanston, Illinois 60208, USA*
[2]*Faculty of Science, Holon Institute of Technology, 58102 Holon, Israel*
[3]*School of Chemistry, Tel-Aviv University, 69978 Tel-Aviv, Israel*

(Received 29 December 2014; accepted 23 March 2015; published online 17 April 2015)

A tight binding model is used to investigate photoinduced tunneling current through a molecular bridge coupled to two semiconductor electrodes. A quantum master equation is developed within a non-Markovian theory based on second-order perturbation theory with respect to the molecule-semiconductor electrode coupling. The spectral functions are generated using a one dimensional alternating bond model, and the coupling between the molecule and the electrodes is expressed through a corresponding correlation function. Since the molecular bridge orbitals are inside the bandgap between the conduction and valence bands, charge carrier tunneling is inhibited in the dark. Subject to the dipole interaction with the laser field, virtual molecular states are generated via the absorption and emission of photons, and new tunneling channels open. Interesting phenomena arising from memory are noted. Such a phenomenon could serve as a switch. © *2015 AIP Publishing LLC.* [http://dx.doi.org/10.1063/1.4917029]

I. INTRODUCTION

Photon-induced coherent tunneling in molecular wires and junctions has been the topic of growing experimental and theoretical activity, fueled by both the new fundamental questions introduced and the premise for long term applications in all-optical device technology.[1–12] The interaction of a molecular junction with an external time-dependent electromagnetic field gives rise to two familiar phenomena that have been proposed as routes to control over the tunneling in molecular wires and quantum dots based on different mechanisms.[13–21] One is photon-assisted tunneling (PAT).[22,23] An external field periodic in time with frequency ω can induce inelastic tunneling events when the electrons exchange energy quanta $\hbar\omega$ with the radiation field. The tunneling occurs through the effective electron density of states at energies $E \pm n\hbar\omega$, which are created by photon absorption ($n > 0$) and emission ($n < 0$) processes. The second well-studied phenomenon is coherent destruction of tunneling (CDT).[24,25] In the presence of a laser field, a pair of the nearest neighbor sites shift up and down in the opposite direction. Mathematically, the quenching of tunneling is a consequence of the proportionality of the effective inter-site tunneling to the Bessel function $J_0(A/\hbar\omega)$, A being the amplitude (with energy unit eV) and ω the frequency of the optical field[18,24–29] and occurs at zeros of the Bessel function.

The inviting variety of new conductance phenomena and control opportunities that light driven junctions introduce come at the cost of new complications. First, light applied to a molecule in contact with a metal surface is much more likely to be absorbed by the substrate than to excite the molecule. The thus excited hot carriers may interact with the molecule and lead to interesting dynamics, but in the process coherence is lost. Second, energy transfer in light driven metal–molecule–metal systems competes with charge transport. References 6 and 30 suggested the use of semiconductor (SC), rather than metal, electrodes as a way of circumventing both problems, noting also several other potential advantages that semiconductor-based molecular electronics may be expected to offer over the more conventional metal-based analog. Whereas the control mechanism of Refs. 6 and 30 relies on laser induced orientation, that of Refs. 31 and 32 uses the photonic replica of the initial state as new transport channels that allow tunneling in the semiconductor-based junction under bias voltages where tunneling does not take place in the dark. Interestingly, Ref. 32 finds that the semiconductor contacts introduce also new conductance phenomena. In particular, the external laser field influences both the coupling between the molecule and the SC electrodes and the inter-site tunneling, with a resulting total net current that depends on the product $J_0(A/\hbar\omega) \times J_1(A/2\hbar\omega)$. As a consequence, the current vanishes at both the roots of $J_0(A/\hbar\omega)$ and those of $J_1(A/2\hbar\omega)$. This phenomenon was termed coherent destruction of induced tunneling (CDIT). The formalism developed in Refs. 31 and 32 allowed a fully analytical solution subject to the Markovian approximation. Memory effects, however, may be expected to play a role in transport junctions. Our goal in the present work is to explore CDIT through a molecule coupled to two semiconductor electrodes using numerical calculations that go beyond the Markovian approximation.

A general Hamiltonian for modeling SC can be expressed as a perturbation of the Newns-Anderson metal model.[34,35] Here, we use one such model, suggested by Koutecký and Davison,[34,48] where both the site energies and the intersite coupling alternate, hence a unit cell includes two sites. The

a)fainberg@hit.ac.il
b)t-seideman@northwestern.edu

Hamiltonian is thus of the form,

$$H_{KD} = \alpha \sum_{j=1}^{N} (|2j-1\rangle\langle 2j-1| - |2j\rangle\langle 2j|) + \sum_{j=1}^{N} (\beta_1 |2j-1\rangle\langle 2j| + \beta_2 |2j\rangle\langle 2j+1| + h.c.) \quad (1)$$

where $|2j-1\rangle$ and $|2j\rangle$ denote two states in j-th unit, α is the site energy, assumed equal in all sites, β_1 is the inter-site coupling within a cell and β_2 is the coupling between two neighbor cells. Analytical expressions for the self energies and the electrodes eigensystems for this model are derived in Ref. 35 and used below. For further numerical treatment, we fit the results of Ref. 35 to several Lorentzians. In the $\alpha \to 0$ case, one obtains a model where only the bonds alternate and in the present work this model is used to describe the semiconductor electrodes. Coupling between the molecule and the SC electrodes is described using second-order perturbation theory, and a quantum reduced master equation (QME) is used to investigate the population dynamics and tunneling current subject to the time dependent external field within an approach based on the time-convolution Nakajima-Zwanzig projection operator formalism. A set of coupled equations for the QME and its auxiliary density matrices are set and numerically solved. This technical method was proposed by Meier and Tannor[36] and was used for master equations based on a time-nonlocal approach in Refs. 36 and 37 and on a time-local one in Refs. 37–42.

In addition, nanojunctions are of interest due to their potential for current gating.[30–32,46,47] Zrenner *et al.*[33] demonstrated that Rabi oscillations between two excitonic energy levels of an InGaAs quantum dot placed in a photodiode can be converted into deterministic photocurrents. This device is based on π-pulse excitation, and can function as an optically triggered single-electron turnstile. However, the main disadvantage of the π-pulse excitation method is the requirement of a resonant light source and the need for precise control over the pulse area. In this relation, we have proposed an optical control method based on the adiabatic rapid passage for enhancing charge transfer in unbiased molecular junctions where the bridging molecule is characterized by a strong charge-transfer transition.[46] The method is robust, being insensitive to the pulse area and the precise location of resonance that makes it suitable for a molecular bridge even for inhomogeneously broadened optical transition. Here, we propose another robust method for the optical control of the charge transferred per pulse. Changing the number of sites N in a molecular bridge, one can realize different types of charge turnstiles.

In Sec. II, we introduce the theory and describe the model. Our results are discussed in Sec. III, where we explore CDIT with a monochromatic laser and consider the case of a short laser pulse. In Sec. IV, we briefly conclude.

II. THEORY

A. Model Hamiltonian

The total Hamiltonian of the system (shown in Fig. 1) describing a molecular bridge including N sites and coupled to two semiconductor electrodes, is given as

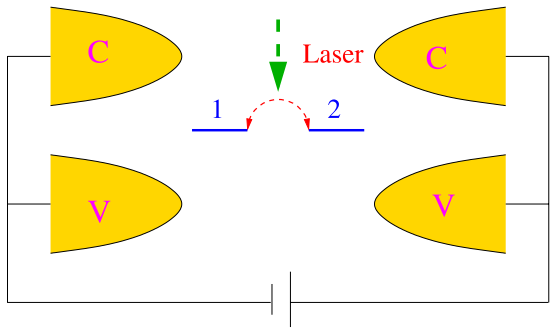

FIG. 1. Scheme of a molecule coupled to semiconductor electrodes, with the total site number N interacting with an external magnetic field (here, N = 2).

$$H = H_S + H_{SC} + V. \quad (2)$$

Here, H_S is the system Hamiltonian including a molecular bridge subject to an external laser field,

$$H_S = H_0 + H_\Delta + H_F(t), \quad (3)$$

where $H_0 + H_\Delta$ is the molecular Hamiltonian and $H_F(t)$ describes the interaction of the bridge sites with the external electromagnetic field $\mathrm{E}(t)$. The first component of the molecular Hamiltonian,

$$H_0 = \sum_{l=1}^{N} \varepsilon_l c_l^\dagger c_l, \quad (4)$$

describes a tight-binding model composed of N sites, where each site represents available orbitals (e.g., the HOMO and/or the LUMO) and ε_l denotes the electron energy on site l. The second component, H_Δ, accounts for electron transfer interactions between the nearest sites within the Huckel model, and is given as

$$H_\Delta = -\sum_{l=1}^{N-1} \Delta (c_{l+1}^\dagger c_l + c_l^\dagger c_{l+1}), \quad (5)$$

where Δ is the inter-site tunneling strength. For a single site ($N = 1$), $H_\Delta = 0$. The last term on the right hand side of Eq. (3) is given by

$$H_F(t) = -\mathbf{D} \cdot \mathrm{E}(t), \quad (6)$$

where

$$\mathrm{E}(t) = A \sin(\omega t), \quad (7)$$

A being the amplitude (a constant in the case of a monochromatic field and a Gaussian function in the case of a pulse) and ω the frequency of the field. The dipole operator, $\mathbf{D}$, is given as

$$\mathbf{D} = \begin{cases} \sum_{l=1}^{N} \frac{2l - N - 1}{2} c_l^\dagger c_l, & N > 1, \\ c_1^\dagger c_1, & N = 1. \end{cases} \quad (8)$$

For the special case N = 1, the system has only one level. It can be taken as a single-level quantum dot. Under the influence of the external laser field, the site shifts up and down, and the laser field acts as a gate voltage.

The second term of Eq. (2), H_{SC}, is the Hamiltonian of intrinsic semiconductor electrodes, expressed as

$$H_{SC} = \sum_{k\in\{L,R\}} (\varepsilon_{ck} c_{ck}^{\dagger} c_{ck} + \varepsilon_{vk} c_{vk}^{\dagger} c_{vk}) \tag{9}$$

that may be obtained from Eq. (1) (see Appendix B). Here, the operators $c_{ck}^{\dagger}$ (c_{ck}) and $c_{vk}^{\dagger}$ (c_{vk}) are the creation (annihilation) operators for electrons with energies $\varepsilon_{c,k}$ and $\varepsilon_{v,k}$ respectively, c and v denote the conduction and valence bands, and $L(R)$ stands for the right (left) lead. Equation (9) is written in the energy representation for the SC, while Eq. (1) is written in the real space. The last term of Eq. (2), V, is the coupling between the molecule and the semiconductor contacts and is responsible for net current in the biased junction,

$$V = \sum_{l=1,N;k\in\{L,R\}} (V_{lck} c_{ck}^{\dagger} c_l + V_{lvk} c_{vk}^{\dagger} c_l) + h.c., \tag{10}$$

where $h.c.$ denotes Hermite conjugate.

B. QME

For application below, it is convenient to rewrite Eq. (10) as

$$V = V_L + V_R, \tag{11}$$

where V_L (V_R) describes the coupling between the electrode and the left (right) edge site of the molecule. Thus,

$$V_L = \sum_{k\in L} (V_{1ck} c_{ck}^{\dagger} c_1 + V_{1vk} c_{vk}^{\dagger} c_1) + h.c. \tag{12}$$

and V_R is obtained by changing the index L into R, and index 1 into N in Eq. (12). We proceed by rewriting V_L as

$$V_L = \sum_{x=1,2} K_x \Phi_x \tag{13}$$

with $K_1 = c_1^{\dagger}$, $K_2 = c_1$, $\Phi_1 = \sum_{k\in L}(V_{1ck}^{*} c_{ck} + V_{1vk}^{*} c_{vk})$ and $\Phi_2 = \sum_{k\in L}(V_{1ck} c_{ck}^{\dagger} + V_{1vk} c_{vk}^{\dagger})$.

In the derivations below, only the left lead will be considered but the formalism has to be applied to the right lead as well. Thus, a quantum master equation describing the electron transfer between the left side semiconductor and the molecule can be expressed as[18,23,37,45]

$$i\hbar \frac{\partial \rho(t)}{\partial t} = [H_S, \rho(t)] - i\hbar \sum_{x,x'} [K_x, \Lambda_{xx'}(t) - \widehat{\Lambda}_{xx'}(t)], \tag{14}$$

with $x, x' = 1,2$. The time-dependent auxiliary operators for the coupling between the molecule and the semiconductor in Eq. (14) are given by

$$\Lambda_{xx'}(t) = \frac{1}{\hbar} \int_0^t \mathrm{d}t' C_{xx'}(t-t') U_S(t,t') K_{x'} \rho(t'), \tag{15}$$

$$\widehat{\Lambda}_{xx'}(t) = \frac{1}{\hbar} \int_0^t \mathrm{d}t' C_{x'x}^{*}(t-t') U_S(t,t') \rho(t') K_{x'}, \tag{16}$$

where $U_S(t,t')$ is the time evolution operator,

$$U_S(t,t') = T_+ \exp\{-\frac{i}{\hbar} \int_{t'}^t \mathrm{d}\tau \mathcal{L}_S(\tau)\}, \tag{17}$$

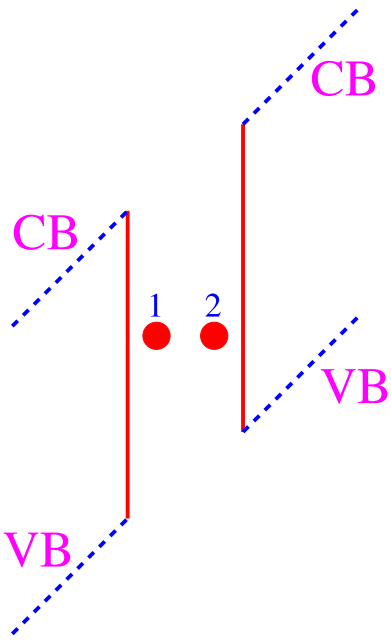

FIG. 2. Slope of the conduction band (CB) and the valence band (VB), due to the applied bias voltage.

with the Liouville operator $\mathcal{L}_S(\tau) = [H_S(\tau), \bullet]$ and time-ordering operator T_+.[37]

C. CDIT and the first photonic replica

We consider a junction consisting of a molecule in contact with two semiconductor electrodes that is subject to bias voltage, as schematically depicted in Fig. 2. In the dark, the barriers between the molecular bridge and the conduction (CB) and valence bands (VB) are too broad to permit tunneling current through the molecule from the valence to the conduction band. In the presence of the external laser field, photoinduced virtual levels with energies $\varepsilon \pm n\hbar\omega$ are generated via photon absorption and emission processes. These levels introduce new, narrow-barrier channels for tunneling current, thus generating effective coupling between the molecule and the semiconductor electrode. The electrode is enhanced compared to the field-free coupling and expresses itself via the last term on the right side of Eq. (14).

This qualitative picture is quantified via the rigorous analytical theory of Ref. 32. Here, the time-dependent external laser field $H_F(t)$ is included via the time evolution operator $U_S(t,t)$, Eq. (17). Under the approximation that the inter-site coupling H_Δ is small compared to the photon energy, i.e., $H_\Delta \ll \hbar\omega$, $U_S(t,t)$ can be rewritten as (see Eqs. (12) and (13) of Ref. 43)

$$\langle l|U_S(t,t')|n\rangle = \mathrm{e}^{-iZ_{l,n}[\sin(\omega t)-\sin(\omega t')]} \times \langle l|\mathrm{e}^{-i\bar{H}_S(t-t')/\hbar} \bullet \mathrm{e}^{i\bar{H}_S(t-t')/\hbar}|n\rangle, \tag{18}$$

where $\bar{H}_S = H_0 + H_\Delta$ is time-independent part of the system Hamiltonian H_S, and $Z_{l,n} = (D_{l,l} - D_{n,n})\mathrm{E}(t)$ is the difference between the energies induced by the dipole operator D at sites l and n. Using the relation $e^{iZ\sin\theta} = \sum_{s=-\infty}^{s=\infty} J_s(Z) e^{is\theta}$, Eq. (18)

can be rewritten as

$$\langle l|U_S(t,t')|n\rangle = \sum_{s=-\infty}^{s=\infty} |J_s(Z_{l,n}/\omega)|^2 e^{-is\omega(t-t')} \times \langle l|e^{-i\bar{H}_S(t-t')/\hbar} \bullet e^{i\bar{H}_S(t-t')/\hbar}|n\rangle. \quad (19)$$

The last expansion holds only when E(t) is a slow function of time, i.e., when the pulse duration significantly exceeds the optical period of the field.[43] Here, the Bessel functions play the role of the amplitudes of the photo-induced virtual levels, where the $s = 0$ term is associated with the field-free molecular state, whereas the $s = \pm 1$ terms are associated with the one photon absorption and emission processes. In the energy representation with the eigenvectors $|\nu\rangle$ and $|\mu\rangle$, the term on the right hand side of Eq. (19) is given as

$$\langle \nu|e^{-i\bar{H}_S(t-t')/\hbar} \bullet e^{i\bar{H}_S(t-t')/\hbar}|\mu\rangle = \langle \nu| \bullet |\mu\rangle e^{-i\omega_{\nu,\mu}t}, \quad (20)$$

where $\omega_{\nu,\mu}$ is the energy difference between the eigenvalues corresponding to the eigenvectors $|\nu\rangle$ and $|\mu\rangle$.

Under the conditions considered here, (see Fig. 2), the spectral density functions become asymmetric only near the first photonic replica. Near the second and higher photonic replica the spectral density functions remain symmetric, and they show influence on the population dynamics. Only the first photonic replica with energies $\varepsilon \pm \hbar\omega$ contribute to the total current. Here, we assume that the above phenomena will take place in the presence of the applied voltage bias inducing the slopes of the conduction and valence bands. This applied bias will not generate any more influence to the current-voltage characteristics. Due to the short distance between the electrodes, the electric field generated from the voltage bias can be ignored and will not affect the site energies.

D. Spectral densities for semiconductor electrodes

The free bath correlation functions, $C_{xx'}(t)$ in Eqs. (15) and (16) are expressed as

$$C_{xx'}(t) = \mathrm{tr}_R\{e^{iH_{SC}t/\hbar}\Phi_x e^{-iH_{SC}t/\hbar}\Phi_{x'}\rho_K\}. \quad (21)$$

For the coupling between the CB and the molecule, the correlation functions are

$$C_{12}(t) = \sum_k |V_{1ck}|^2 n_F(-\hbar\omega_k + E^F_{Lc})e^{-i\omega_k t}, \quad (22)$$

$$C_{21}(t) = \sum_k |V_{1ck}|^2 n_F(\hbar\omega_k - E^F_{Lc})e^{i\omega_k t}, \quad (23)$$

where n_F is the Fermi function, and E^F_{Lc} is the Fermi level of the CB. The latter correlation functions can be expressed in terms of a spectral density function J_{Lc} as

$$C_{12}(t) = \int_{-\infty}^{\infty} \frac{d\omega}{2\pi} J_{Lc}(\omega)\, n_F(-\hbar\omega + E^F_{Lc})e^{-i\omega t}, \quad (24)$$

$$C_{21}(t) = \int_{-\infty}^{\infty} \frac{d\omega}{2\pi} J_{Lc}(\omega)\, n_F(\hbar\omega - E^F_{Lc})e^{i\omega t}. \quad (25)$$

Here, we use the alternating bonds model Eq. (1) to describe the semiconductor electrodes. Analytical expressions for the spectral densities within this model are derived in Ref. 35, reading

$$J_{Lc}(\omega) = \Gamma_{Lc}\sqrt{\frac{[(\beta_1+\beta_2)^2 - (\hbar\omega)^2][(\hbar\omega)^2 - (\beta_1-\beta_2)^2]}{(\hbar\omega)^2}}, \quad \text{with} \quad |\beta_1 - \beta_2| < \hbar\omega < |\beta_1 + \beta_2|, \quad (26)$$

$$J_{Rv}(\omega) = \Gamma_{Rv}\sqrt{\frac{[(\beta_1+\beta_2)^2 - (\hbar\omega)^2][(\hbar\omega)^2 - (\beta_1-\beta_2)^2]}{(\hbar\omega)^2}}, \quad \text{with} \quad -|\beta_1 + \beta_2| < \hbar\omega < -|\beta_1 - \beta_2|. \quad (27)$$

Here, β_1 and β_2 are the alternate bond coupling parameters, $2|\beta_1 - \beta_2|$ is the material band gap, and $|\beta_1 + \beta_2| - |\beta_1 - \beta_2|$ is the bandwidth of the valence band and conduction band. Finally, Γ_{Lc} and Γ_{Rv} are coupling strengths, to be specified below as functions of β_1, β_2, V_{1ck}, and V_{2vk}.

In order to compute the electron transport process using the Non-Markovian theory of Refs. 37 and 44, we require a numerically more convenient form than Eqs. (26) and (27) for the spectral functions, so as to simplify the time integration in Eqs. (15) and (16). Here we fit the spectral density of Ref. 35 to several Lorentzians as

$$J_{Lc}(\omega) = \Gamma_{Lc}\sum_{j=1}^{N_j} \frac{\alpha_j}{(\hbar\omega - \Omega_j)^2 + \Gamma_j^2}, \quad (28)$$

$$J_{Rv}(\omega) = \Gamma_{Rv}\sum_{j=1}^{N_j} \frac{\alpha_j}{(\hbar\omega + \Omega_j)^2 + \Gamma_j^2}. \quad (29)$$

When $\Gamma_{Lc} = \Gamma_{Rv}$, J_{Lc} and J_{Rv} are related by reflection symmetry about $\omega = 0$.

Inserting Eqs. (28) and (29) into Eqs. (24) and (25), and using Residue theorem, we find that the correlation functions C_{12} and C_{21} are given as

$$C_{12}(t) = \Gamma_{Lc}\sum_{j=1}^{N_j} \frac{\alpha_j}{\Gamma_j}\left(n_F(-\Pi_k^- + E_F)e^{-i\Pi_k^- t}\right) - \frac{2i}{\beta}\sum_{k=1}^{N'_j} J_{Lc}(\nu_k^*)e^{-i\nu_k^* t}, \quad (30)$$

$$C_{21}(t) = \Gamma_{Lc}\sum_{j=1}^{N_j}\left(n_F(\Pi_k^+ - E_F)e^{i\Pi_k^+ t}\right) - \frac{2i}{\beta}\sum_{k=1}^{N'_j} J_{Lc}(\nu_k)e^{i\nu_k t}. \quad (31)$$

Here, the abbreviations $\Pi_k^{\pm}$ stand for $\Omega_k \pm i\Gamma_k$ and the Matsubara frequencies ν_k are equal to $i\frac{2\pi k+\pi}{\beta} + E_{Lc}^F$.

E. Current operator and on-site population

Under the influence of the applied voltage bias, electrons can tunnel through the molecular bridge and we adopt the standard convention where electrons tunnel from the left to the right electrode. The operator of the electron number at the left semiconductor lead related to the electron tunneling is expressed as $N_l = \sum_{k\in L}(c_{ck}^\dagger c_{ck} + c_{vk}^\dagger c_{vk})$, with the summation performed over the reservoir degrees of freedom. The current from the left lead to the wire is given by Refs. 18, 23, and 45,

$$\begin{aligned} I_l(t) &= e\frac{\mathrm{d}}{\mathrm{d}t}\mathrm{tr}\{N_l\rho(t)\} = -ie\,\mathrm{tr}\{[N_l, H(t)]\rho(t)\} \\ &= \mathrm{tr}\{\mathcal{I}_l(t)\rho(t)\}, \end{aligned} \tag{32}$$

where e denotes the elementary charge ($e > 0$), and $\mathcal{I}_l$ is the current operator of the left electrode. The latter operator is given by

$$\mathcal{I}_l(t)\rho(t) = e\left[\Lambda_{12}(t)c_1^\dagger - c_1^\dagger\widehat{\Lambda}_{12}(t) + c_1\widehat{\Lambda}_{21}(t) - \Lambda_{21}(t)c_1\right], \tag{33}$$

and the total transient current through the molecular junction is $I(t) = (I_l(t) - I_r(t))/2$, $I_R(t)$ being the current from the right electrode to the wire.

The on-site population at time t,

$$P_l(t) = \mathrm{tr}\{c_l^\dagger c_l\rho(t)\}, \tag{34}$$

exhibits oscillations, as does also the current $I(t)$ due to the external laser field. Their averaged (or long time limit) values $\bar{I}$ and $\bar{P}_l$ that are time-dependent, are obtained by averaging over 6 periods as

$$\bar{\mathrm{G}}(t) = \frac{1}{6\Delta T}\int_{t-3\Delta T}^{t+3\Delta T} d\tau \mathrm{G}(\tau)\,. \tag{35}$$

Here, ΔT is the dynamic period of the system, which is mostly dependent on the inter-site coupling Δ. G $= I, P_l$. The averaged values $\bar{I}$ and $\bar{P}_l$ will be used in the following discussion.

The transferred charge per pulse can be obtained via the integration of the current as

$$Q = \int_0^\infty I dt, \tag{36}$$

this charge can be measured experimentally.

III. RESULTS AND DISCUSSION

In this section, we study numerically the phenomenon of CDIT both in the case of a CW laser (Eq. (7)) and in that of a short pulse laser with its amplitude assumed to vary as a Gaussian function of time. We set the site energies to $E_l = 0$ and the inter-site coupling to $\Delta = 0.04$ eV for all sites, and the coupling between the molecular and the semiconductor leads is set to $\Gamma_{Lc} = \Gamma_{Rv} = 0.01$ eV. $I_0 = e \times 0.01$ eV$/\hbar$ $= 2.45 \times 10^{-6}$ A is taken as the unit of tunneling current. We explore the cases of a single site ($N = 1$), a pair of sites ($N = 2$) and multi-site ($N > 2$) bridges with the parameters $\beta_1 = -1.60$, $\beta_2 = -2.185$, used in Ref. 35 to correspond to a silicon lead. 16 Lorentzian functions are used to fit the functions $J_{Lc}(\omega)$ and $J_{Rv}(\omega)$ with the parameters listed in Table I (see the Appendix A). The bandwidth is 3.2 eV, and the band gap is 1.17 eV. The Fermi energies are assumed to be in the middle of the bandgap, the VBs of both sides are occupied, and the CBs are empty. The temperature is taken to be $T = 0$.

TABLE I. Parameters of the 16 Lorentz fitting functions.

	ω_j	Ω_j	Γ_j
j = 1	2.677 28	1.194 36	0.952 616
j = 2	2.495 77	3.296 48	1.300 22
j = 3	−0.962 7	3.815 17	0.155 423
j = 4	−1.804 35	4.302 38	1.354 33
j = 5	−1.304 67	3.805 28	0.143 08
j = 6	0.092 392 5	0.653 22	0.148 371
j = 7	−1.367 82	0.602 339	0.104 405
j = 8	3.460 58	0.599 3	0.094 452 5
j = 9	2.535 23	0.790 877	0.579 307
j = 10	2.579 98	2.169 73	1.261 14
j = 11	2.251 06	3.808 82	0.148 062
j = 12	−4.444 96	0.736 11	0.716 136
j = 13	−2.201 52	0.598 172	0.090 756 1
j = 14	0.000 174 406	0.605 044	0.019 192 1
j = 15	0.000 892 279	3.751 77	0.058 646 4
j = 16	−0.103 057	4.051 52	0.441 333

A. CW source

In the presence of a laser field, upper and lower photon-assisted virtual states are generated through the absorption and emission of photons, respectively. Consequently, charge tunnels between the molecular bridge and semiconductor electrodes. In this section, a monochromatic laser is applied to investigate the tunneling current, on-site population, and CDIT.

As discussed earlier, the spectral density functions become asymmetric only near the first photonic replica. Hence, only the first photonic replication-assisted tunneling contributes to the net current. As shown in Eq. (19) (Ref. 32), its amplitude is defined by the first order Bessel function $J_1(A/\hbar\omega)$ with the roots 0, 3.832, 7.016, 10.17, ... When A$/\hbar\omega$ coincides with a root, the coupling between the bridge and the first order photonic replication vanished and with it also the current - a phenomenon introduced in Refs. 31 and 32 and coined CDIT to note its analogy to the well studied effect of CDT. In a multiple-site system, the time-dependent dipole energies depend not only on the coupling between the molecule and the semiconductor lead, but also on the inter-site tunneling matrix element Δ between two nearest-neighbor sites. Here, the nearest neighbor sites energies shift up and down in the opposite direction. The effective inter-site coupling is determined by the zero-order Bessel function, J_0,[1,24,25]

$$\Delta_{eff} = \Delta J_0(A/\hbar\omega). \tag{37}$$

That is induced from the dipole energy difference between the nearest neighbor sites and is determined by the amplitude and

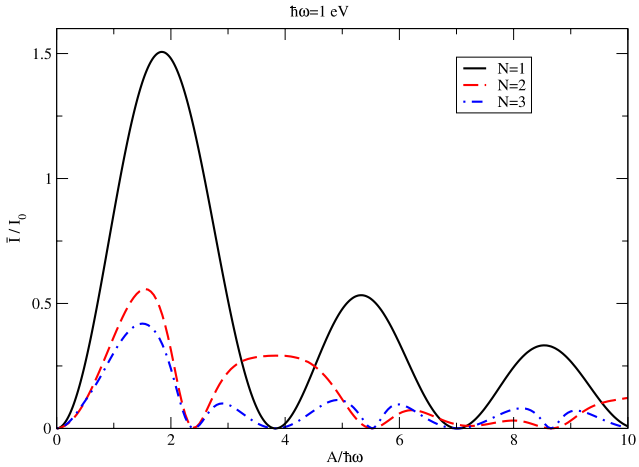

FIG. 3. Average current $\bar{I}$ in the long time limit shown as a function of the ratio of the amplitude and frequency $A/\hbar\omega$ of a CW laser (Eq. (7)).

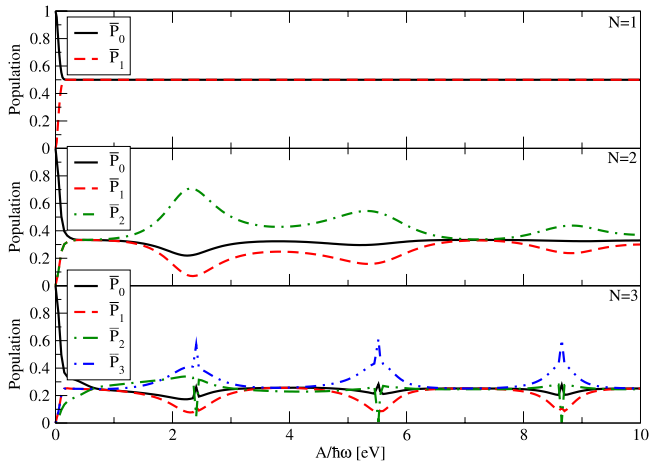

FIG. 4. Average population in the long time limit shown as a function of the ratio of the amplitude and frequency of the incident laser field $A/\hbar\omega$ (Eq. (7)).

frequency of the field (Eq. (7)). When $A/\hbar\omega$ matches a root of the zero-order Bessel function, 2.405, 5.520, 8.653, ..., the effective tunneling parameter vanishes and with it also the effective tunneling between the nearest neighbor sites. Here the population is localized at the edge site, corresponding to the CDIT.

The dipole energies influence not only the coupling between the molecule and the semiconductor contacts, but also the inter-site coupling between the two nearest neighbor sites within the molecule. The diagonal elements of the dipole operator are (1), (1/2, −1/2), (1, 0, −1) for (N = 1, 2, 3), respectively. The dipole induced energy difference between the edge sites and the electrodes (dipole energy is zero) increases with the site number, and hence the positions of CDIT due to J_1 changes. In the single site system and the three site system, the difference is 1, whereas in the double site system it is 1/2. In the multiple-site bridge, the difference between the nearest neighbor sites is 1, and CDIT due to J_0 occurs always at the same point. The tunneling currents are determined by the products $J_1(A/\omega)$, $J_0(A/\hbar\omega)J_1(A/2\hbar\omega)$ and $J_0(A/\hbar\omega)J_1(A/\hbar\omega)$ for $N = 1,2$, and 3, respectively.

Figure 3 shows the average tunneling current $\bar{I}$ vs. the ratio $A/\hbar\omega$. In all cases (N = 1, 2, 3), CDIT is seen at roots of J_1. CDIT is seen at roots of J_0 only for N = 2, 3. At these roots, the tunneling currents becomes zero. Their relative population distribution is shown in Fig. 4. At CDIT arising from the roots of J_0, population is localized on the edge site with P_2 (in case with N = 2) or P_3 (in case with N = 3), reaching their maximal value, respectively. However, this value is not 1. This is because of the second and higher photonic replica. They are symmetric and not contributing to the total net currents, but they do influence the population dynamics. At CDIT arising from the roots of J_1, population tunneling from the electrode to the molecule via this virtual channel is inhibited, however the other channels are still open. The time-dependent on-site populations are shown in Fig. 5. For multisites (N = 2, 3) populations show oscillation behavior due to the coherence of the non-diagonal elements of the density matrix.

Because of the photon-assisted tunneling, virtual levels $E + n\hbar\omega$ or $E - n\hbar\omega$ are generated through the photon absorption or emission processes, respectively. The probabilities of both processes are given by the square of the Bessel functions $J_n(A/\hbar\omega)$, and therefore, are equal to each other. In a single site system, these virtual levels are additional channels for the tunneling current. In a two-site system, virtual levels will be generated for each site, and show oscillation behavior (due to the dipole operator). All these virtual levels make contribution to the tunneling current.

For the multi-site bridges (N = 4, 5), the two diagonal elements of the dipole operator D for the two edge sites are (3/2, −3/2) and (2, −2), respectively, corresponding to the maximum and the minimum values in D. The difference between the edge sites and the electrodes (dipole energy is zero) increases with the number of sites, hence CDIT occurs at the points that are 2/3, 1/2 of the root of the $J_1(A/\hbar\omega)$. The difference between the two nearest neighbor diagonal elements, which are relative to the nearest neighbor sites, remains unified, hence CDIT occurs at the roots of J_0, as shown in Fig. 6.

B. CDIT by a short laser pulse

In this subsection, a short laser pulse is applied to investigate the tunneling current. Its time-dependent amplitude

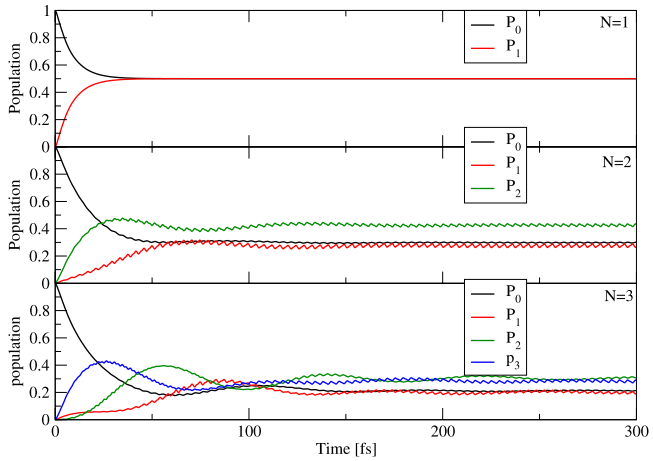

FIG. 5. Populations shown as a function of time. $A = 1.6$ eV (Eq. (7)).

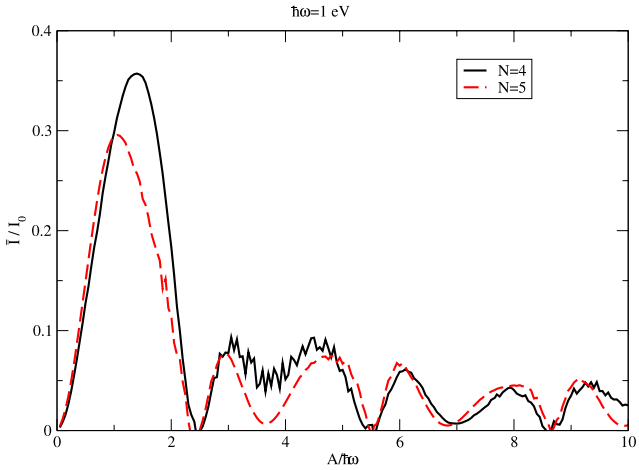

FIG. 6. Averaged current $\bar{I}$ in the long time limit shown as a function of the ratio of the incident field amplitude and frequency, $A/\hbar\omega$ (Eq. (7)).

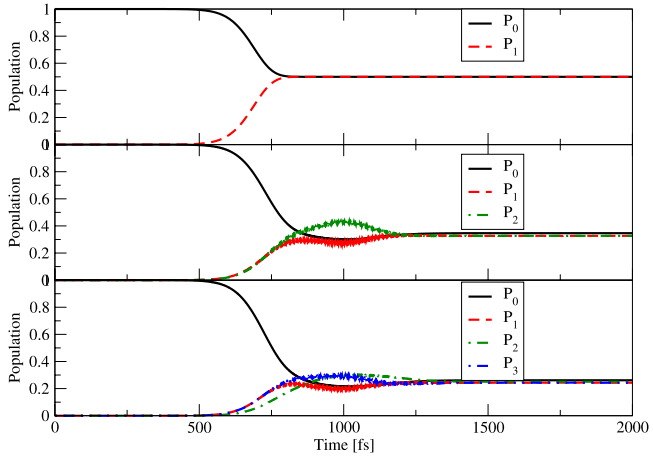

FIG. 8. Populations vs time in the presence of a Gaussian laser field with an amplitude $A_0 = 1.6$ eV (Eq. (38)). From top to bottom, $N = 1, 2, 3$.

has a Gaussian envelope,

$$\mathrm{E}(t) = A(t)\sin(\omega t), \tag{38}$$

$$A(t) = A_0 \exp[-(t-t_0)^2/2\sigma^2], \tag{39}$$

with parameters $t_0 = 1000$ fs and $\sigma = 100$ fs. As the pulse turns on, the first photonic replication-assisted tunneling begins to contribute. The first order Bessel function J_1 (describing the tunneling between the molecule and the electrodes for the first photonic replication) begins to increase from 0, and population begins to tunnel from the electrode to the molecule.

Fig. 7 shows the time evolution of the net current. The current reaches its maximal values around the time when the Gaussian envelope, and likewise the Bessel function J_1, reach their maximum value. The relative populations are shown in Fig. 8. Population begins to tunnel from the electrode to the molecule when the amplitude reaches a certain value. Subsequently, the short pulse disappears, the coupling between the electrode and the molecule returns to zero, and tunneling is inhibited, while some population localize on the molecule.

Fig. 9 shows a rather complex behavior with two different laser amplitude, $A_0 = 2.405$ and $A_0 = 3.832$, with the relative values $A_0/\hbar\omega$ being the root of the Bessel function J_0 and J_1, respectively. With increasing time-dependent amplitude, several peaks and minima appear due to the combination of J_1 and J_0. These peaks and minima correspond to the certain time-dependent amplitude $A(t)$ of the incoming laser field. All the line shapes first reach their peak value, determined by J_1, then begin to drop until the Gaussian pulse envelope reaches their maximum values. In the left panel, the cases with N = 2 and N = 3 reach their zero values when $A(t)$ reaches its maximal value 2.405. While in the right panel, when $A(t)$ reaches its maximal value 2.405, cases with N = 2 and N = 3 reaches their first drop. After that the case with N = 1 reaches its zero values when $A(t)$ reaches its maximal value 3.832, and the case with N = 3 reaches its second drop.

In our numerical simulation, the inter-site coupling parameter was 0.04 eV that corresponded to an oscillation with the period of 100 fs. At the same time, the oscillator behavior generated from the electric field is much faster (e.g., the period is 2 fs for the amplitude A = 2 eV). This explains the oscillations shown in these figures.

Fig. 10 shows the transferred charge Q/e per pulse where e is the charge of one electron. This value changes with the

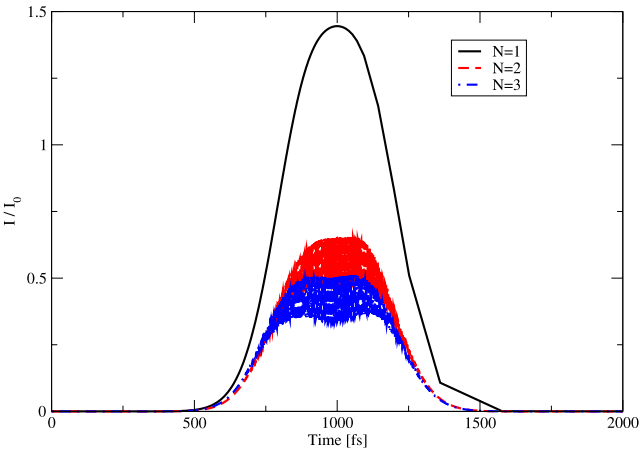

FIG. 7. Current $I(t)$ vs time in the presence of a Gaussian laser pulse with amplitude $A_0 = 1.6$ eV (Eq. (38)). The red dashed line is enlarged by 1.5.

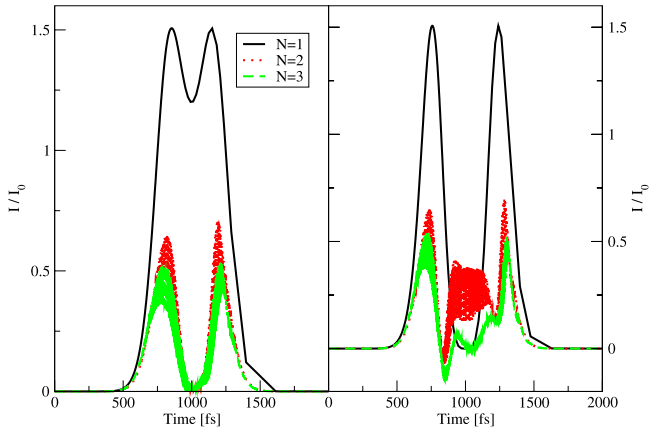

FIG. 9. Time-dependent current I(t) in the presence of a Gaussian laser pulse with the amplitude $A_0 = 2.405$ eV (left panel) and $A_0 = 3.832$ eV (right panel) (Eq. (38)). The red dashed line is enlarged by 1.5.

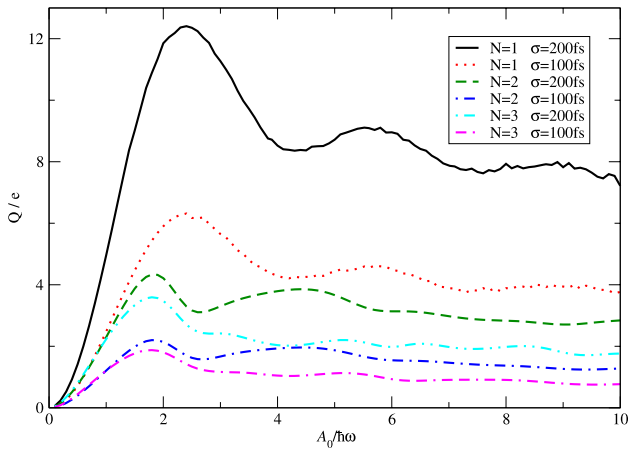

FIG. 10. The transferred charge number Q/e is shown as a function of the amplitude A_0 of the Gaussian laser pulse and its bandwidth σ.

amplitude A of the Gaussian laser pulse, its bandwidth σ, and depends on the number of sites N in the molecular bridge. One can see that the transferred charge Q per pulse is close to e for N = 3, A > 6 and σ = 100 fs. The effect is robust, and the system performs as an optically triggered single-electron turnstile device in this case. In spite of the small charge transferred per pulse (e), the effect may be measured. In the experiment they use a train of short laser pulses and measure a time-integrated photocurrent I = ef where f is the pulse repetition frequency.[33] For f = 82 MHz, they obtain a time-integrated current I of 13.1 pa that may be measured.[33]

IV. CONCLUSION

In this paper, in contrast to Refs. 31 and 32 we use a tight binding model to investigate the tunneling current through a molecular bridge coupled to two semiconductor electrodes. Via the quantum master equation, the non-Markovian effects are investigated in the presence of time-dependent laser field. Dealing with the spectral density and accounting the coupling between the molecular bridge and the electrodes, Bessel functions are generated numerically (see Eq. (19)), which are photonic replica of the molecular states and show a good picture of the influence of the external laser field. The photonic replication assisted tunneling through a molecular bridge coupled to SC electrodes is investigated within a QME. The coupling between the molecule and the SC electrodes is included within the second-order perturbation theory. The population dynamics and current tunneling process are examined via a non-Markovian framework in the presence of the external laser field. Our SC Hamiltonian is based on a one-dimensional alternating bond model, for which the spectral density describing the coupling between the molecule and the SC electrodes was determined analytically in our previous work.[35] Several Lorentzian functions are used to fit this spectral function for further numerical treatment. Due to the interesting property that the density of states in the energy gap between the VB and CB vanishes, population tunneling between the molecule and the SC electrodes is inhibited in the dark even under the influence of bias voltage. In the presence of the external laser field, many virtual channels are introduced via exchange of energy quanta $\hbar\omega$ with the external field. These PAT channels can facilitate the transfer through the molecule. We consider conditions under which only transport mediated by the first photonic replica (energetically displaced by $\pm\omega$ with respect to the initial energy level) contribute, where the coupling strength between the molecule and the semiconductor electrodes can be expressed in terms of the Bessel function J_1.

The semiconductor electrodes have not only the advantages of circumventing substrate mediated dynamics, which hinders optical control in the case of metal-based molecular junctions, offering stronger chemical bonding to organic molecules and fitting within the existing device technology. In addition, they also introduce several interesting transport phenomena. The laser field influences both the coupling between the molecule and the SC electrodes and the inter-site tunneling. Nearest neighbor site energies are raised and lowered out of phase with one another, and the effective tunneling parameter is given by a Bessel function J_0. For the single site, the tunneling current is determined by J_1, and CDIT occurs when J_1 reaches zero. For a multiple-site bridge, the tunneling current is determined by the product $J_0 \times J_1$, and CDIT occurs at roots of either J_0 or J_1 reaches zero.

In the case of a short pulse laser, we find that during the pulse turn-on, the coupling between the molecule and the electrode (expressed by the J_1), and the effective inter-site tunneling (expressed by the J_0) increase and subsequently exhibit oscillations bounded by the Gaussian envelope. After the pulse turn-off, tunneling between the molecule and the electrode is inhibited while part of the population is left on the molecule. Such a phenomenon may find application for optical switching. We have also shown that the molecular nanojunction with semiconductor electrodes can perform as an optically triggered single-electron turnstile device.

ACKNOWLEDGMENTS

We thank the Northwestern-Tel Aviv University Exchange Program for support of a visit of B.F. to Northwestern University, in the framework of which this research was carried

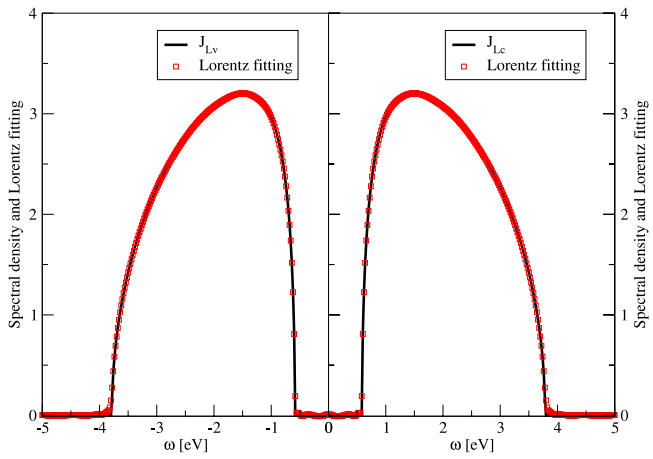

FIG. 11. Spectral density functions J_{Lc} and J_{Lv} as a function of energy ω, together with their fits to Lorentzian functions.

out. T.S. is grateful to the National Science Foundation (Grant No. CHE-1012207) and the Department of Energy (Grant No. DE-SC0001785) for support. B.F. is grateful to the Israel-US Binational Science Foundation for support.

APPENDIX A: FITTING THE SPECTRAL DENSITY FUNCTIONS USING LORENTZIAN FUNCTIONS

Figure 11 shows the spectral density functions $J_{Lc}(\omega)$ and $J_{Lv}(\omega)$, together with their fit to Lorentzian functions, which are seen to match well. As shown by Eqs. (26) and (27), the spectral densities are non-zero at energies inside the band. 16 Lorentz functions are used to obtain the fitting with the parameters shown in the Table I.

APPENDIX B: DIAGONALIZATION OF HAMILTONIAN FOR THE MODEL, SUGGESTED BY KOUTECKY AND DAVISON

Here, we present the derivation of Hamiltonian, Eq. (9), from Hamiltonian, Eq. (1). The eigenstates of Hamiltonian, Eq. (1), are given by Eq. (21) of Ref. 35,

$$|k_n\rangle = A_{k_n} \sum_{j=1}^{N} \frac{\{\beta_1 \sin(2k_n j) + \beta_2 \sin[2k_n(j-1)]\}|2j-1\rangle + (\varepsilon_{k_n} - \alpha)\sin(2k_n j)|2j\rangle}{\sqrt{(\varepsilon_{k_n} - \alpha)^2 + \beta_1^2 + \beta_2^2 + 2\beta_1\beta_2\cos(2k_n)}}, \tag{B1}$$

where A_{k_n} is the normalization constant, ε_{k_n} are the eigenstates of H_{KD} given by Eq. (18) of Ref. 35, and k is quantized by $\beta_1 \sin[2k_n(N+1)] + \beta_2 \sin(2k_n N) = 0$ with $n = 1, 2, \ldots, 2N$. Then, the Hamiltonian of the semiconductor electrodes may be written in the diagonal form as

$$H'_{SC} = \sum_{k_n \in \{L,R\}} \varepsilon_{k_n} |k_n\rangle\langle k_n|. \tag{B2}$$

Hamiltonian, Eq. (B2), is written in the first quantization picture. Going to the second quantization picture, we replace the Dirac states by creation and annihilation operator, and get Eq. (9).

[1]S. Kohler and P. Hänggi, Nat. Nanotechnol. **2**, 675 (2007).
[2]J. R. Heath, Annu. Rev. Mater. Res. **39**, 1 (2009).
[3]F. Chen and N. J. Tao, Acc. Chem. Res. **42**, 573 (2009).
[4]J. C. Cuevas and E. Scheer, *Molecular Electronics: An Introduction to Theory and Experiment* (World Scientific Publishing Co. Inc., New Jersey, 2010).
[5]D. C. Guhr, D. Rettinger, J. Boneberg, A. Erbe, P. Leiderer, and E. Scheer, Phys. Rev. Lett. **99**, 086801 (2007).
[6]M. G. Reuter, M. Sukharev, and T. Seideman, Phys. Rev. Lett. **101**, 208303 (2008).
[7]E. G. Petrov, Y. V. Shevchenko, V. May, and P. Hänggi, J. Chem. Phys. **134**, 204701 (2011).
[8]U. Peskin and M. Galperin, J. Chem. Phys. **136**, 044107 (2012).
[9]R. Arielly, A. Ofarim, G. Noy, and Y. Selzer, Nano Lett. **11**, 2968 (2011).
[10]M. Galperin, M. A. Ratner, and A. Nitzan, Nano Lett. **9**, 758 (2009).
[11]G.-Q. Li, B. D. Fainberg, A. Nitzan, S. Kohler, and P. Hänggi, Phys. Rev. B **81**, 165310 (2010).
[12]G.-Q. Li, M. S. Shishodia, B. D. Fainberg, B. Apter, M. Oren, A. Nitzan, and M. A. Ratner, Nano Letters **12**, 2228 (2012).
[13]B. Popescu, P. B. Woiczikowski, M. Elstner, and U. Kleinekathöfer, Phys. Rev. Lett. **109**, 176802 (2012).
[14]Y. Selzer and U. Peskin, J. Phys. Chem. C **117**, 22369 (2013).
[15]M. Kornbluth, A. Nitzan, and T. Seideman, J. Chem. Phys. **138**, 174707 (2013).
[16]B. A. Ashwell, S. Ramakrishna, and T. Seideman, J. Phys. Chem. C **117**, 22391 (2013).
[17]C. E. Creffield and G. Platero, Phys. Rev. B **69**, 165312 (2004).
[18]S. Welack, M. Schreiber, and U. Kleinekathöfer, J. Chem. Phys. **124**, 044712 (2006).
[19]E. Cota, R. Aguado, and G. Platero, Phys. Rev. Lett. **94**, 107202 (2005).
[20]M. Galperin and A. Nitzan, Phys. Rev. Lett. **95**, 206802 (2005).
[21]T. Brandes, Phys. Status Solidi B **243**, 2293 (2006).
[22]G. Platero and R. Aguado, Phys. Rep. **395**, 1 (2004).
[23]G.-Q. Li, M. Schreiber, and U. Kleinekathöfer, EPL **79**, 27006 (2007).
[24]S. Kohler, J. Lehmann, and P. Hänggi, Phys. Rep. **406**, 379 (2005).
[25]S. Kohler, S. Camalet, M. Strass, J. Lehmann, G.-L. Ingold, and P. Hänggi, Chem. Phys. **296**, 243 (2004).
[26]S. Camalet, J. Lehmann, S. Kohler, and P. Hänggi, Phys. Rev. Lett. **90**, 210602 (2003).
[27]S. Camalet, S. Kohler, and P. Hänggi, Phys. Rev. B **70**, 155326 (2004).
[28]L. Wang and V. May, Phys. Chem. Chem. Phys. **13**, 8755 (2011).
[29]L. Wang and V. May, J. Electroanal. Chem. **660**, 320 (2011).
[30]M. G. Reuter, M. A. Ratner, and T. Seideman, Phys. Rev. A **86**, 013426 (2012).
[31]B. D. Fainberg and T. Seideman, Phys. Status Solidi A **209**, 2433 (2012).
[32]B. D. Fainberg and T. Seideman, Chem. Phys. Lett. **576**, 1 (2013).
[33]A. Zrenner, E. Beham, S. Stufler, F. Findeis, M. Bichler, and G. Abstreiter, Nature **418**, 612 (2002).
[34]J. Koutecký, *Quantum Chemistry of Crystal Surfaces*, in Advances in Chemical Physics, edited by I. Prigogine (John Wiley & Sons, 1965), Vol. 9.
[35]M. G. Reuter, T. Hansen, T. Seideman, and M. A. Ratner, J. Phys. Chem. A **113**, 4665 (2009).
[36]C. Meier and D. J. Tannor, J. Chem. Phys. **111**, 3365 (1999).
[37]U. Kleinekathöfer, J. Chem. Phys. **121**, 2505 (2004).
[38]Y. J. Yan and R.-X. Xu, Annu. Rev. Phys. Chem. **56**, 187 (2005).
[39]B. D. Fainberg, P. Hanggi, S. Kohler, and A. Nitzan, AIP Conf. Proc. **1147**, 78–86 (2009); e-print arXiv: 0902.0134 (cond-mat.mes-hall).
[40]S. Kohler, J. Lehmann, and P. Hanggi, Phys. Rep. **406**, 379 (2005).
[41]F. J. Kaiser, M. Strass, S. Kohler, and P. Hanggi, Chem. Phys. **322**, 193 (2006).
[42]U. Kleinekathöfer, G.-Q. Li, S. Welack, and M. Schreiber, EPL **75**, 139 (2006).
[43]B. D. Fainberg, V. A. Gorbunov, and S. H. Lin, Chem. Phys. **307**, 77 (2004).
[44]B. Fainberg, "Ultrafast dynamics and non-Markovian processes in four-photon spectroscopy," in *Advances in Multi-Photon Processes and Spectroscopy (Part 3)*, edited by H. Lin, A. A. Villaeys, and Y. Fujimura (World Scientific, Singapore, 2003).
[45]G.-Q. Li, M. Schreiber, and U. Kleinekathöfer, New J. Phys. **10**, 085005 (2008).
[46]B. D. Fainberg, M. Jouravlev, and A. Nitzan, Phys. Rev. B. **76**, 245329 (2007).
[47]B. D. Fainberg and A. Nitzan, Phys. Status Solidi A **206**, 948 (2009).
[48]E. N. Foo and S. G. Davison, Surf. Sci. **55**, 274 (1976).